URSI AP-RASC, Sydney, Australia, 17 – 22 August 2025

Accurate Ray-Path Modeling for Wide-Angle Multi-Beam Flat GRIN Lens Design

Li-Zhao Song*(1), Pei-Yuan Qin (1), and Y. Jay Guo (1)
(1) Global Big Data Technologies Centre (GBDTC), University of Technology Sydney (UTS), Australia

Abstract

In this study, we present an innovative design methodology for gradient-index (GRIN) lenses engineered to generate multiple beams from distinct focal points. Comprehensive numerical investigations reveal that the current state-of-the-art multi-beam lens design, synthesized on the assumption of linear and parallel ray paths, suffers from ray-path errors that limit its applicability to lenses of arbitrary dimensions. To address these constraints, a more accurate synthesis technique is proposed, providing general formulas applicable to a wide variety of lens profiles. Comparative analyses between the conventional and the new method demonstrate that the latter achieves enhanced realized gains consistently for all multiple beams over a broad frequency range. Experimental validation was carried out using a 3D-printed lens featuring seven independent beams in an angular range of ±44°. The measured gain variations between multiple beams remain below 2.93 dB across the 12.3-19 GHz band.

1. Introduction

Lens antennas have garnered significant interest for their high gain and wide bandwidth, making them ideal for reliable long-distance wireless communication. However, their inherently narrow beamwidths often restrict the overall signal coverage. This limitation has spurred extensive research into multi-beam lenses, which promise simultaneous and stable communications with spatially dispersed targets. To this end, a variety of lens geometries and configurations have emerged, including the spherical Luneburg lens [1], the 2-D geodesic lens [2], and the flat GRIN lens [3]. Notably, flat GRIN lenses are particularly advantageous due to their broad 2-D beam coverage, lightweight construction, and ease of integration into existing systems.

So far, the synthesis of multi-beam flat GRIN lenses has primarily employed transformation optics and geometrical optics. For example, the work in [4] utilized transformation optics to convert the permittivity and permeability of a 3-D spherical Luneburg lens into a 2-D planar distribution, thus preserving its multi-beam properties in a flat form. By repositioning the feed antenna relative to the lens aperture, beam scanning ranges between ±32° and ±35° were achieved for two orthogonal linear polarizations, with a peak aperture efficiency of 46.2%. In another study [5], a different transformation technique was developed to expand the beam coverage to ±54°, albeit at the expense of reducing the aperture efficiency to 21.2%. Additionally, a millimeter-wave full-dielectric lens was introduced in [6] through direct ray-path analysis based on geometrical optics. By moving the feed antenna along the focal plane, a 2-D beam coverage of ±30° in both azimuth and elevation planes was realized, achieving an aperture efficiency as high as 76.3%. Similarly, a design based on geometrical optics and feed displacement in [7] achieved a wide angular coverage of ±60° with aperture efficiencies reaching up to 35%. From these state-of-the-art designs, it is noticed that a trade-off exists between beam coverage and efficiency, that is, extending beam coverage beyond ±40° typically results in decreased aperture efficiency. To address this trade-off, a novel multi-beam synthesis method based on geometrical optics was proposed in [8], offering beam coverage of ±45° in two orthogonal planes with a peak aperture efficiency of 66.4%. However, this method relies on the assumption of linearly parallel ray paths within the lens. This assumption is valid only for thin GRIN lenses. As the lens thickness increases, the approximation introduces significant ray-path errors, thereby degrading multi-beam performance.

In this work, we conduct comprehensive and accurate analyses of ray paths in flat GRIN lenses for multi-beam synthesis for the first time. We numerically investigate the ray-path errors associated with the synthesis method described in [8], which helps to underscore the limitations of its underlying assumptions. Building upon these insights, we introduce a new synthesis process for multi-beam flat GRIN lenses that effectively mitigates ray-path errors and overcomes the constraints of previous methods. This novel approach not only significantly enhances gain performance for multiple beams across a broad frequency range but also doubles the gain bandwidth while simplifying the overall configuration through the integration of multiple compact feed antennas.

2. Ray-Path Modeling for Multi-Beam GRIN Lens Design

To obtain multi-beam flat GRIN lenses with wide angular coverages, a typical method is to synthesize a symmetrical lens aperture for generating oblique beams at two extreme angles, supported by conjugate offset foci. Figure 1(a) illustrates the synthesis configuration developed in [8]. Two feeding sources, positioned at A and B, illuminate the lens to enable beam radiations at ±β. To simplify the derivation of the refractive-index profile on the lens aperture, the ray paths inside the lens were approximated as linear and parallel, with a slope equal to tan β. For a lens with thickness d, radius a, and offset focal length l_0, the refractive-index profile on the lens with respect to the radial coordinate ρ was obtained as

$$n(\rho) = 1 + \frac{\sqrt{{l_0}^2+a^2(cos\beta)^2} - \sqrt{{l_0}^2+\rho^2(cos\beta)^2}}{d/cos\beta}. \qquad (1)$$

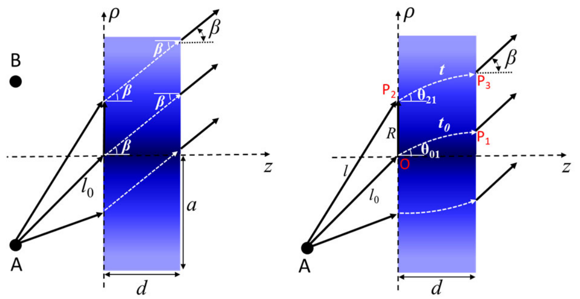

(a) (b)

Figure 1. Multi-beam flat GRIN lens. (a) Approximated ray-path modeling in [8]. (b) Accurate ray-path modeling.

However, due to the radially varying refractive indices on the lens, the actual internal ray paths should follow curved trajectories as illustrated in Figure 1(b), and satisfy an accurate ray-congruence equation of

$$l_0 + \int_0^{P_1} n(\rho)\, dt_0 + (R_{p3} - R_{p1}) sin\beta = l + \int_{P_2}^{P_3} n(\rho)\, dt, \qquad (2)$$

where t_0 and t represent the internal ray paths; R_{P3} and R_{P1} denote the radii at the exit points; l_0 and l are the focal distances of two incident points. The conservation of momentum and Snell's law can be applied to reformulate (2) as

$$l_0 + \int_0^{R_{p1}} \sqrt{n^2(\rho) - (n(0)cos\theta_{01})^2}\, d\rho + dn(0)cos\theta_{01} + (R_{p3} - R_{p1}) sin\beta = l + \int_R^{R_{p3}} \sqrt{n^2(\rho) - (n(R)cos\theta_{21})^2}\, d\rho + dn(R)cos\theta_{21}, \qquad (3)$$

where all utilized variables are marked in Figure 1(b). Due to limited space, detailed derivation process will be shared during the conference.

To examine the ray-path errors of the approximated solution using (1), the left and right sides of the actual ray-congruence equation of (3) are denoted as Ls and Rs, respectively. Then, by replacing n(ρ) in (3) with (1), the ray-path errors are characterized as

$$Error(\rho) = \frac{|Ls - Rs|}{Ls}. \qquad (4)$$

Based on the above process, we evaluated a flat GRIN lens model using the reported synthesis method in [8] at 13 GHz. The design parameters are β=45°, a=2.5λ₀, l_0=3.75λ₀, and d=0.75λ₀. Figure 2(a) displays the computed ray-path errors, showing a peak value of 6.8%. Notably, an incongruence region appears in the range –0.5<ρ/a<0, where no solutions for the ray-path errors can be obtained because the ideal exit points corresponding to the actual ray trajectories are absent on the synthesized lens. Consequently, a portion of the lens aperture fails to contribute to the intended beam formation, thereby degrading the overall radiation performance.

To further illustrate the behavior of ray-path errors across various lens designs, we compiled the maximum errors as a function of lens thickness and focal length while keeping the lens radius fixed at a = 2.5λ_0, as shown in Figure 2(b). It is evident that as the lens becomes thicker, a substantial incongruence area develops. This is primarily because the assumption of linear, parallel ray paths in [8] increasingly deviates from the actual trajectories in thicker lens profiles.

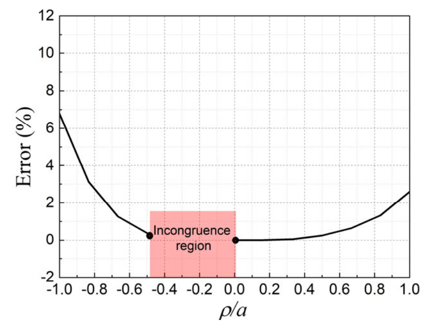

(a)

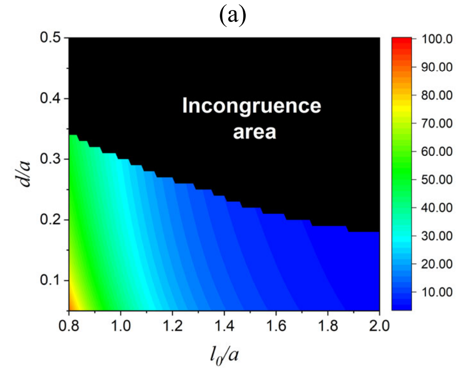

(b)

Figure 2. Ray-path errors of multi-beam flat GRIN lenses using the method in [8]. (a) A selected design. (b) Maximum errors of different designs with variable d and l_0.

3. New Multi-Beam GRIN Lens Design

To address the errors of the reported method in [8], we propose a new multi-beam synthesis approach. As shown in Figure 3, the trajectories of the rays within the lens vary based on their entry points and differ from the output beam angle β. For ease of numerical analysis, we continue to assume that the rays travel in straight lines. Under these conditions, a new simplified ray-congruence equation is obtained as

$$l_0 + n(0)\frac{d}{\cos(\theta_{01})} + sin\beta(d\tan(\theta_{21}) + R - dtan\theta_{01}) =$$

$$l + n(R)\frac{d}{\cos(\theta_{21})}. \qquad (5)$$

To determine the refractive index at the center of the lens, n(0), we set the index at point P_3 to unity whenever point P_2 is located at the lens boundary; in other words, n(R_{p3}) equals 1 when R=a. Consequently, the refractive index n(R) for any point at a radius R can be uniquely determined using (5).

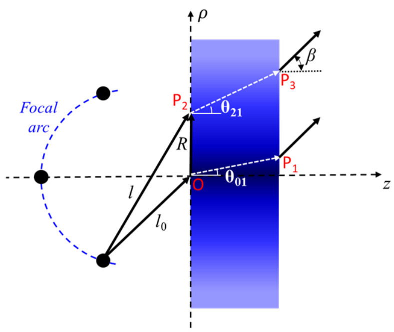

Figure 3. New proposed ray-path modeling for multi-beam GRIN lens.

To validate the proposed approach, we designed a flat GRIN lens with the same physical parameters utilized in Section 2. The ray-path errors are evaluated using the procedure outlined in that section and are presented in Figure 4(a) alongside a comparison with the method in [8]. Notably, the new synthesis method eliminates the incongruence region and reduces the maximum ray-path error to only 2%. In addition, Figure 4(b) summarizes the maximum ray-path errors for various lens parameters, clearly showing that the incongruence region has been substantially minimized, highlighting the new method's versatility for different lens designs.

To further demonstrate the improved radiation performance with the new proposed method, two multi-beam lens prototypes, denoted as Lens A and Lens B, were developed in ANSYS HFSS using the same physical parameters. Lens A was created following the state-of-the-art design method presented in [8], whereas Lens B's refractive-index profile was determined using (5). Subsequently, the ray-path errors for a boresight beam were also analyzed over a range of focal distances, leading to an optimal focal position with minimal error. As shown in Figure 3, the selection of three focal points forms a focal arc along which multiple feed antennas can be positioned to produce distinct beams. Simulated beam patterns for Lenses A and B are shown in Figure 5(a) and (b), respectively, with Lens B delivering higher realized gains across all beams. Figure 5(c) and (d) compare the peak gain versus frequency for the boresight beam and the most oblique beam from both lenses, demonstrating that the new proposed method consistently provides significant gain improvements over a broad operating bandwidth.

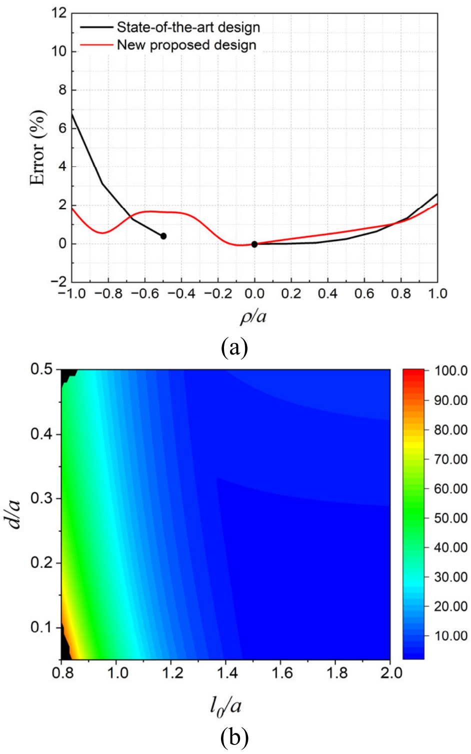

Figure 4. Ray-path errors of the new proposed method. (a) Comparison with state-of-the-art design. (b) Maximum errors of different lenses with variable d and l_0.

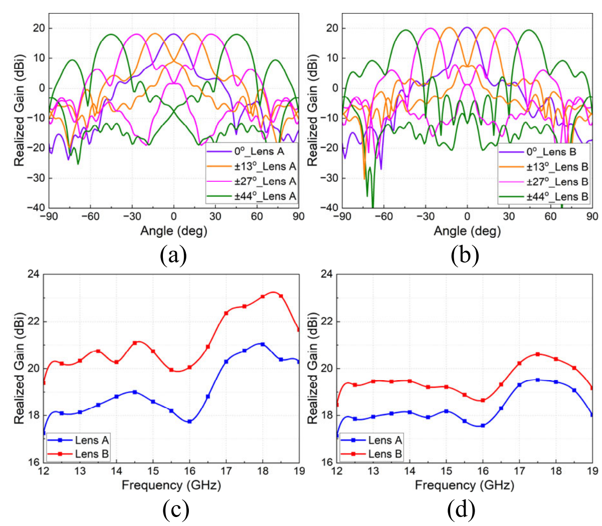

Figure 5. (a) Multi-beam patterns of Lens A. (b) Multi-beam patterns of Lens B. (c) Comparison of peak boresight realized gains. (d) Comparison of realized gains at the largest oblique beams (±44°).

4. Fabrication and Experiment

As a proof of concept, we fabricated Lens B from Section 3 using Fortify's advanced 3D printing technology with Rogers Radix printable material (dielectric constant 2.8). Figure 6 shows the implemented prototype. Seven patch array antennas were arranged along the focal arc to serve as feed sources for the multiple beams. The measured radiation patterns at various frequencies within the operating band are presented in Figure 7, demonstrating a wide beam coverage of ±44° with less than 3-dB gain drops. The wide-angle multi-beam performance has been maintained in a wide frequency range, with a 3-dB gain bandwidth of 42.8% between 12.3 and 19 GHz.

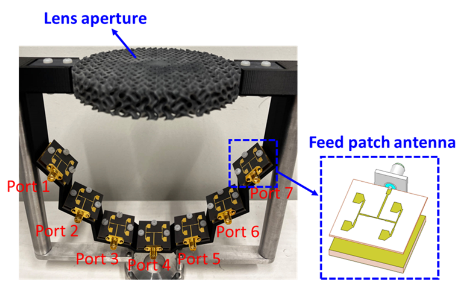

Figure 6. Implemented multi-beam flat GRIN lens prototype.

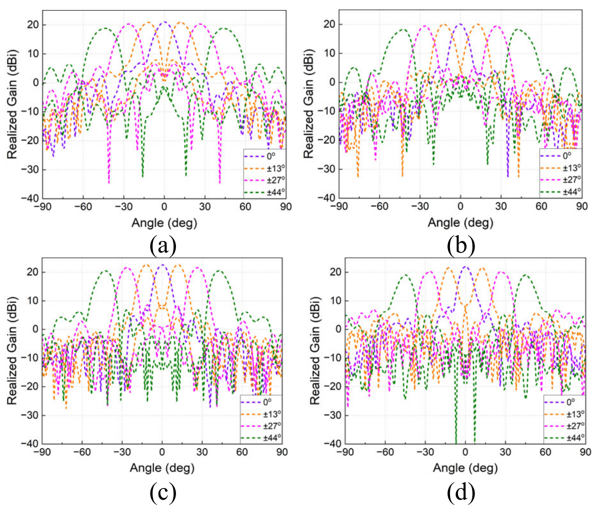

Figure 7. Measured multi-beam patterns of Lens B. (a) 13 GHz. (b) 15 GHz. (c) 17 GHz. (d) 19GHz.

6. Conclusion

This study introduces an innovative synthesis approach for multi-beam flat GRIN lenses that effectively minimizes the ray-path errors observed in earlier designs. Accurate analyses of the ray trajectories within the lens enable the generation of multi-focal, multi-beam radiations. Moreover, the new method significantly enhances the overall radiation performance, with solid validations through simulation and measurement.

References

[1] M. Ansari, B. Jones and Y. J. Guo, "Spherical Luneburg lens of layered structure with low anisotropy and low cost," *IEEE Trans. Antennas Propag.*, **70**, 6, June 2022, pp. 4307-4318, doi: 10.1109/TAP.2022.3140509.

[2] Q. Liao, N. J. G. Fonseca and O. Quevedo-Teruel, "Compact multibeam fully metallic geodesic Luneburg lens antenna based on non-Euclidean transformation optics," *IEEE Trans. Antennas Propag.*, **66**, 12, December 2018, pp. 7383-7388, doi: 10.1109/TAP.2018.2872766.

[3] D. Jia, Y. He, N. Ding, J. Zhou, B. Du and W. Zhang, "Beam-steering flat lens antenna based on multilayer gradient index metamaterials," *IEEE Antennas Wireless Propag. Lett.*, **17**, 8, August 2018, pp. 1510-1514, doi: 10.1109/LAWP.2018.2851442.

[4] Y. Su and Z. N. Chen, "A flat dual-polarized transformation-optics beamscanning Luneburg lens antenna using PCB-stacked gradient index metamaterials," *IEEE Trans. Antennas Propag.*, **66**, 10, October 2018, pp. 5088-5097, doi: 10.1109/TAP.2018.2858209.

[5] Y. Su, Z. N. Chen, "A radial transformation-optics mapping for flat ultra-wide-angle dual-polarized stacked GRIN MTM Luneburg lens antenna," *IEEE Trans. Antennas Propag.*, **67**, 5, May 2019, pp. 2961-2970, doi: 10.1109/TAP.2019.2900346.

[6] J. Melendro-Jimenez, P. Sanchez-Olivares, A. Tamayo-Dominguez, X. Sun and J. M. Fernandez-Gonzalez, "3D printed directive beam-steering antenna based on gradient index flat lens with an integrated polarizer for dual circular polarization at W-band," *IEEE Trans. Antennas Propag.*, **71**, 1, January 2023, pp. 1059-1064, doi: 10.1109/TAP.2022.3217177.

[7] H. -F. Wang, Z. -B. Wang, Z. -H. Wu and Y. -R. Zhang, "Beam-scanning lens antenna based on elliptical paraboloid phase distribution metasurfaces," *IEEE Antennas Wireless Propag.* Lett., **18**, 8, August 2019, pp. 1562-1566, doi: 10.1109/LAWP.2019.2922695.

[8] L. -Z. Song, M. Ansari, P. -Y. Qin, S. Maci, J. Du and Y. J. Guo, "Two-dimensional wide-angle multibeam flat GRIN lens with a high aperture efficiency," *IEEE Trans. Antennas Propag.*, **71**, 10, October 2023, pp. 8018-8029, doi: 10.1109/TAP.2023.3298143.